Supporting Information

A Thermally Reversible Dynamic Bond as a Magnetic and Nonlinear Optical Switch

Xue-Li Cao,[1,2,3]† Jin Liu,[1,2,3]† Chuan-Qi Shen,[1,2] Shu-Qi Wu,[4]* Zi-Shuo Yao,[5] Qing Li,[1,2,3] Zhong-Min Cao,[1,2,3] Lu-Yao Liu,[1,2,3] Fu-Lin Lin,[1,2] Zi-Ang Nan,[1,2] Zhu Zhuo,[1,2] Wei Wang,[1,2] Osamu Sato,[4] and You-Gui Huang[1,2,3]*

[1]*State Key Laboratory of Structure Chemistry, Fujian Institute of Research on the Structure of Matter, Chinese Academy of Science, Fuzhou, Fujian, 350002, China*
[2]*Fujian Science & Technology Innovation Laboratory for Optoelectronic Information of China*
[3]*Xiamen Key Laboratory of Rare Earth Photoelectric Functional Materials, Xiamen Institute of Rare Earth Materials, Haixi Institutes, Chinese Academy of Sciences, Xiamen, Fujian, 361021, China*
[4]*Institute for Materials Chemistry and Engineering & IRCCS, Kyushu University, 744 Motooka, Nishi-ku, Fukuoka, Japan*
[5]*Key Laboratory of Cluster Science of Ministry of Education, School of Chemistry and Chemical Engineering, Beijing Institute of Technology, Beijing, China*

Table of contents

S1. Materials and Methods

S1.1 Starting materials

The ligand H_4BPTC (biphenyl-3,3',5,5'-tetracarboxylic acid) was prepared according to the procedure reported in literature[S1]. All other reagents were purchased from commercial sources and used without purification.

S1.2 Physical measurements

The IR spectrum was recorded in the range 500–4000 cm^{-1} on a JASCO FT/IR-600 Plus spectrometer. Thermogravimetric analyses (TGA) was performed using a TG/DTA6300 system at a rate of 10 °C/min. Powder X-ray diffraction (PXRD) patterns were obtained on a Rigaku 2100 diffractometer using Cu-*K*α radiation with flat plate geometry. DSC curves were measured on a NETZSCH DSC 300 at a rate of 5 °C/min, and the heat capacity measurement was performed on a PPMS (MODEL 6000) magnetometer at a rate of 5 °C/min. Magnetic measurements were performed on a MPMS-5S SQUID magnetometer. The gas adsorption/desorption measurements were performed on an Autosorb-iQ automatic gas adsorption instrument. Before the experiments, the sample was degassed under reduced pressure (< 10^{-2} Pa) at 100 °C for 3 h. The SHG properties were measured using the Kurtz-Perry method with a Q-switched Nd:YAG laser (1044 nm). Elemental analysis (EA) data were obtained with an Elementar Vario EL Cube.

S1.3 Crystallography

Single-crystal X-ray data were harvested on a Bruker D8 Venture diffractometer with Mo-K_α radiation. Structures were solved usinga direct method and refined by the full-matrix least-squares technique on F^2 with SHELXTL 2014 program.[S2] The hydrogen atoms are geometrically generated and refined using a riding model. The PLATON/SQUEEZE procedures[S3] were used to treat the disordered solvents in the voids of the structures of **1·solvent**. The two-component inversion twin strategy was used to refine the structures of the low temperature (LT) phases. The X-ray crystallographic coordinates for structures reported in this article have been deposited at the Cambridge Crystallographic Data Centre (CCDC), under deposition numbers CCDC 2412727−2412728 and 2323611−2323616. These data can be obtained free of charge from The Cambridge Crystallographic Data Centre via www.ccdc.cam.ac.uk/data_request/cif. Detail crystallographic data are listed in Table S1, S2 and S3.

S1.4 Calculation of the isosteric heat of adsorption (Q_{st}).

$$\ln P = \ln N + \sum_{i=0}^{m} a_i N^i + \sum_{i=0}^{n} \binom{n}{k} b_i N^i$$

$$Q_{ST} = -R \sum_{i=0}^{m} a_i N^i$$

A virial-type expression of the above form was used to fit the combined isotherm data of desolvated **1** for CO_2 at 273 and 298 K, where P is the pressure described in mmHg, N is the adsorbed amount in mg/g, T is the temperature in K, a_i and b_i are virial coefficients, and m and n are the number of coefficients used to describe the isotherms. Q_{st} is the coverage-dependent heat of adsorption and R is the universal gas constant.

S1.5 Evaluation of the non-covalent interactions and calculation dipolar moment.

The non-covalent interactions[S4] within the structures have been evaluated by the Multiwfn package[S5], and the quantum chemical calculations have been carried out using

Gaussian 16[S6]. The dipole moments have been calculated by the B3LYP method and 6-31G* basis set.

S1.6 *ab initio* calculations.

All ab initio calculations were performed with the ORCA program package Version 4.1.2[S7,S8]. For all the calculations, the TZVPP basis with the corresponding auxiliary sets (def2-TZVPP/JK) was used[S9,S10]. The initial coordinates obtained high-temperature and low-temperature phase were employed for DFT calculations with constraints. Only the hydrogen atomic positions were optimized at the B3LYP/TZVP level of theory[S11,S12]. Spin-orbit coupling was taken into account using a mean-field spin-orbit coupling operator. The magnetic susceptibility was calculated by the quasi-degenerate perturbation theory in a 5000 Oe external field. The results were projected onto the ligand field scheme by the *ab initio* ligand field analysis implemented in the ORCA package.[S13]

Table S1. Crystallographic data of **1·solvent**.

1	HT phase	LT phase
Formula	$C_{23}H_{14}CoN_3O_4$	$C_{23}H_{14}CoN_3O_4$
Formula weight	455.30	455.30
Temp. (*K*)	328	200
Crystal System	orthorhombic	orthorhombic
Space group	*Fddd*	*Fdd2*
a (Å)	8.7775(15)	57.851(3)
b (Å)	18.411(3)	8.7588(4)
c (Å)	58.630(11)	18.3472(6)
V(Å^3)	9475(3)	9296.6(7)
Z	16	16
$\rho_{cal.}$(g cm^{-3})	1.277	1.301
μ	0.755	0.770
F(000)	3712	3712
Flack		0.48(2)
θ *range* (°)	2.319–27.475	2.329–27.474
Reflections ($I > 2\sigma$)	2192	4219
$R_1(I > 2\sigma)$	0.0710	0.0468
$wR_2(all)$	0.1520	0.1079
GOF on F^2	1.223	1.002
CCDC#	2323611	2323612

[a] $R = \sum||F_0|-|F_c||)/\sum|F_0|$
[b] $wR = |\sum w(F_0-F_c)^2/\sum w(F_0^2)^2|^{1/2}$

Table S2. Crystallographic data of **1·solvent**.

1	LT phase	HT phase
Formula	$C_{23.5}H_{14}CoN_3O_{7.5}$	$C_{23}H_{14}CoN_3O_4$
Formula weight	517.31	455.30
Temp. (*K*)	200	328
Crystal System	orthorhombic	orthorhombic
Space group	*Fdd2*	*Fddd*
a (Å)	57.7432(15)	8.7595(8)
b (Å)	8.7802(2)	18.4634(12)
c (Å)	18.3056(4)	58.264(5)
V(Å^3)	9280.9(4)	9423.0(13)
Z	16	16
$\rho_{cal.}$(g cm^{-3})	1.481	1.284
μ	0.792	0.759
F(000)	4208	3712
Flack	0.407(18)	
θ *range* (°)	2.782–27.522	3.112–27.499
Reflections ($I > 2\sigma$)	4712	2197
$R_1(I > 2\sigma)$	0.0370	0.0364
$wR_2(all)$	0.0951	0.0899
GOF on F^2	1.029	1.060
CCDC#	2412727	2412728

[a] $R = \sum||F_0|-|F_c||)/\sum|F_0|$
[b] $wR = |\sum w(F_0-F_c)^2/\sum w(F_0^2)^2|^{1/2}$

Table S3. Crystallographic data of desolvated **1** during two cooling and heating cycles.

Desolvated **1**	HT phase (270 K)	LT phase (255 K)	HT phase (305 K)	LT phase (260 K)
		→ cooling	→ heating	→ cooling
Formula	$C_{23}H_{14}CoN_3O_4$	$C_{23}H_{14}CoN_3O_4$	$C_{23}H_{14}CoN_3O_4$	$C_{23}H_{14}CoN_3O_4$
Formula weight	455.30	455.30	455.30	455.30
Temp. (*K*)	270	255	305	260
Crystal System	orthorhombic	orthorhombic	orthorhombic	orthorhombic
Space group	*Fddd*	*Fdd2*	*Fddd*	*Fdd2*
a (Å)	8.7459(8)	58.302(6)	8.7560(2)	58.329(10)
b (Å)	18.4031(18)	8.7674(9)	18.4480(6)	8.7744(13)
c (Å)	58.295(6)	18.307(2)	58.302(2)	18.335(3)
V(Å^3)	9382.7(16)	9357.7(19)	9417.5(5)	9384(3)
Z	16	16	16	16
$\rho_{cal.}$(g cm^{-3})	1.289	1.293	1.284	1.289
μ	0.763	0.765	0.760	0.763
F(000)	3712	3712	3712	3712
Flack		0.31(4)		0.45(4)
θ *range* (°)	2.321– 27.546	2.795– 27.582	2.316– 27.499	2.597– 27.685
Reflections ($I > 2\sigma$)	2088	3858	2207	3299
$R_1(I > 2\sigma)$	0.1087	0.0563	0.0471	0.0550
$wR_2(all)$	0.2790	0.1818	0.1119	0.1732
GOF on F^2	1.388	1.082	1.141	1.108
CCDC#	2323613	2323614	2323615	2323616

[a] $R = \sum||F_0|-|F_c||/\sum|F_0|$
[b] $wR = |\sum w(F_0-F_c)^2/\sum w(F_0^2)^2|^{1/2}$

Table S4. Elemental analysis data of **1·solvent**.

	C (%)	H (%)	N (%)
calculate	53.723	4.220	7.998
experiment	53.096	4.184	7.827

Table S5. Spin and orbital contributions to the magnetism.

	spin contribution to *g* value		orbital contribution to *g* value		principle *g* value	
	HT	LT	HT	LT	HT	LT
x	1.767	1.686	0.019	0.028	1.990	1.983
y	2.750	2.525	0.184	0.318	2.286	2.295
z	5.007	5.143	0.257	0.503	2.474	2.540
iso	3.175	3.118	0.153	0.283	2.250	2.273

S2. Synthesis

Synthesis of $Co_2(TPY)_2(BPTC)(CH_3OH)_{0.5}\cdot(H_2O)_3$ (**1·solvent**):

$CoCl_2\cdot 6H_2O$ (0.300 g, 1.25 mmol), TPY (0.250 g, 1.07 mmol), and H_4BPTC (0.150 g, 0.455 mmol) were dissolved with MeOH (80 mL) in a Teflon-lined autoclave. The autoclave was sealed and heated at 150 °C for 1 day and then cooled to room temperature. Pink hexagonal prism crystals of **1·solvent** were harvested by filtration (0.015 g, Yield: 86.2%).

S3. Structures, characterizations and physical properties.

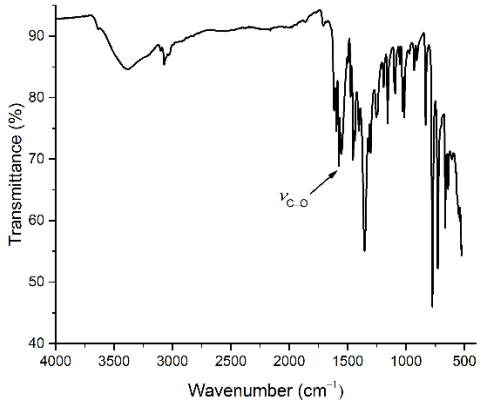

Figure S1. IR spectrum of **1·solvent**. The absorption at 1574 cm^{-1} can be assigned to the $\upsilon_{C=O}$ of $BPTC^{4-}$.

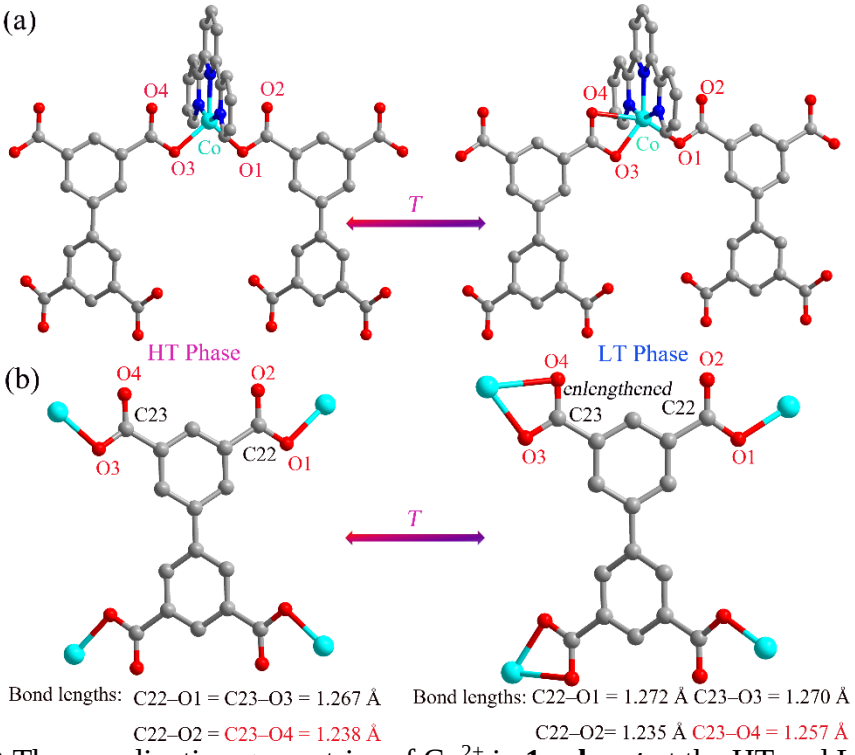

Figure S2. (a) The coordination geometries of Co^{2+} in **1·solvent** at the HT and LT phases. (b) The coordination geometries of $BPTC^{4-}$ in **1·solvent** at the HT and LT phases.

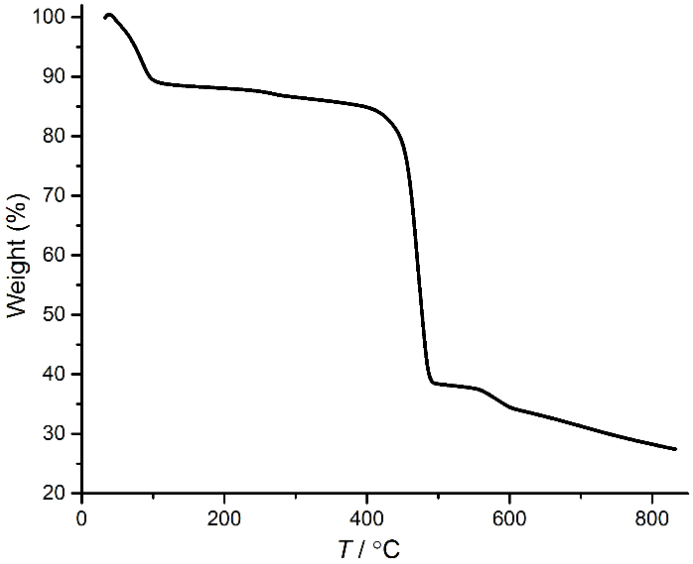

Figure S3. TGA for **1·solvent**. TG analysis of shows a weight loss of ca. 10.52 wt% from 30 to 100 °C which corresponds to the loss solvent molecules.

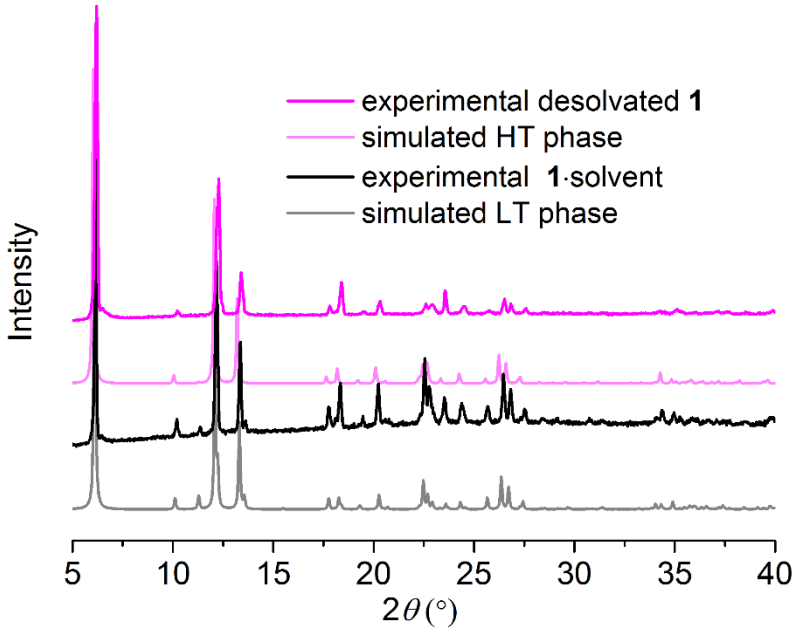

Figure S4. PXRD patterns of **1·solvent** and **1**. The experimental PXRD patterns for both **1·solvent** and **1** were obtained at room temperature. The experimental PXRD pattern for **1·solvent** matches well with the simulated pattern of LT phase. For the sample after desolvation, both LT and HT phases probably exist leading to the slight mismatch with both the simulated PXRD patterns. This result is probably caused by the broad temperature range of the phase transition.

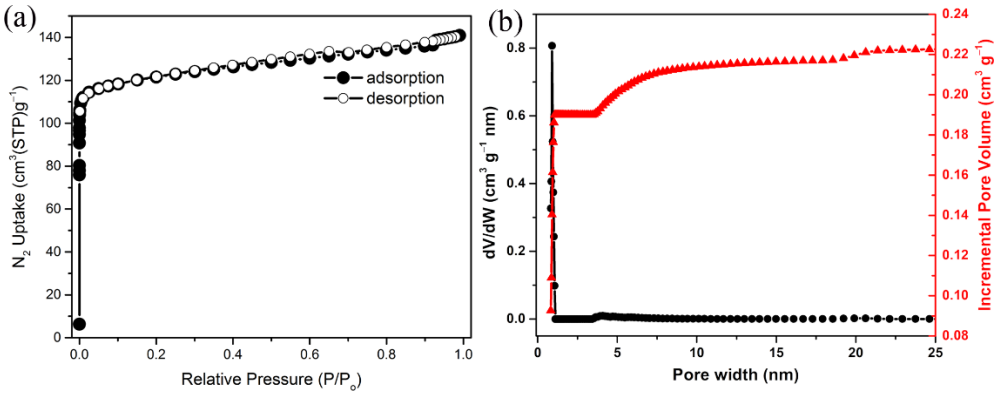

Figure S5. (a) The N_2 sorption data of **1** at 77 K. (b) Pore size distribution of **1**. The pore volume was calculated based on the N_2 uptake at $P/P°$ = 0.96, and the pore size distribution was extracted with the Non-Local Density Functional Theory (NLDFT) method[S14].

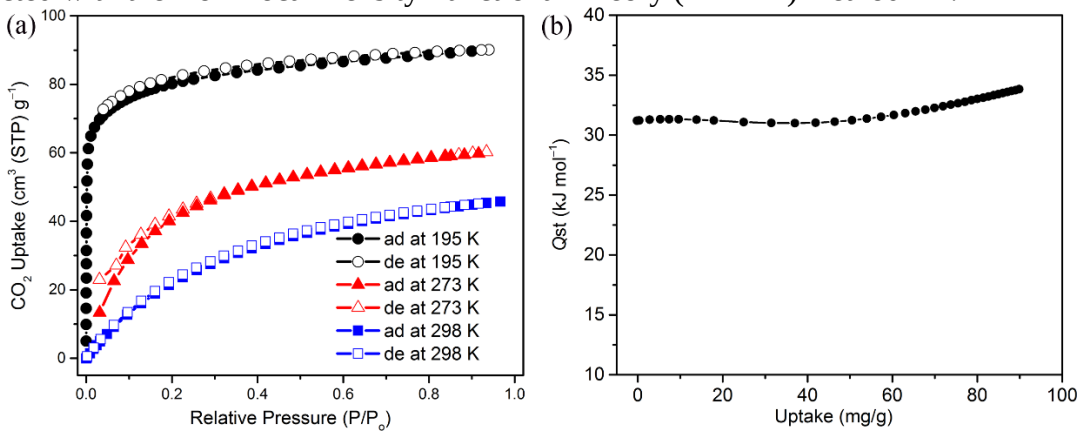

Figure S6. (a) The CO_2 adsorption isotherms of **1** at 195, 273, and 298 K. (b) The isosteric heat of adsorption (Q_{st}) of **1** for CO_2 (The data was obtained based on the isotherms at 273 and 298 K).

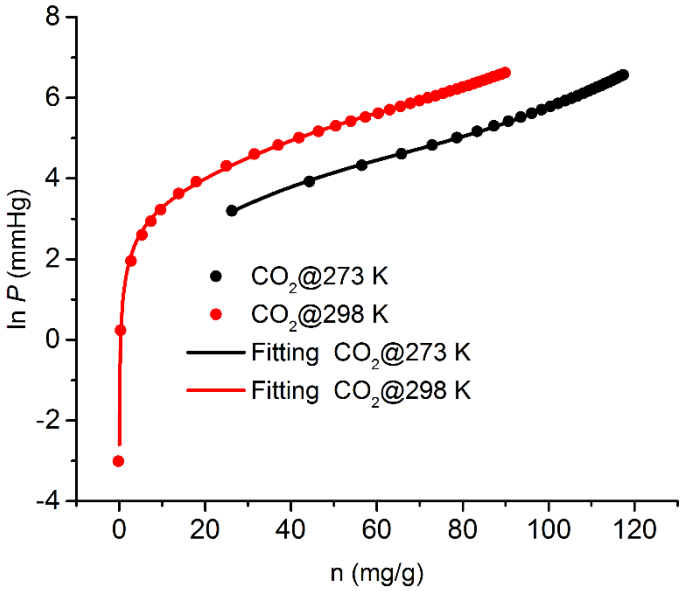

Figure S7. The virial fitting of the adsorption of **1** towards CO_2.

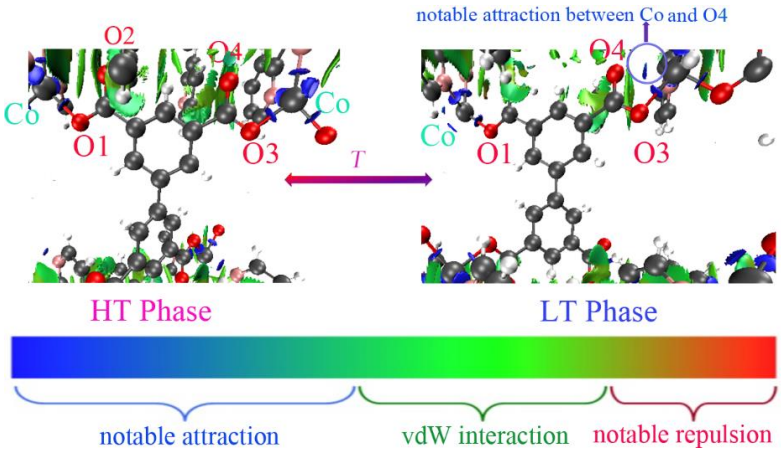

Figure S8. The Co–O4 interactions in the HT and LT phases evaluated by quantum calculation.

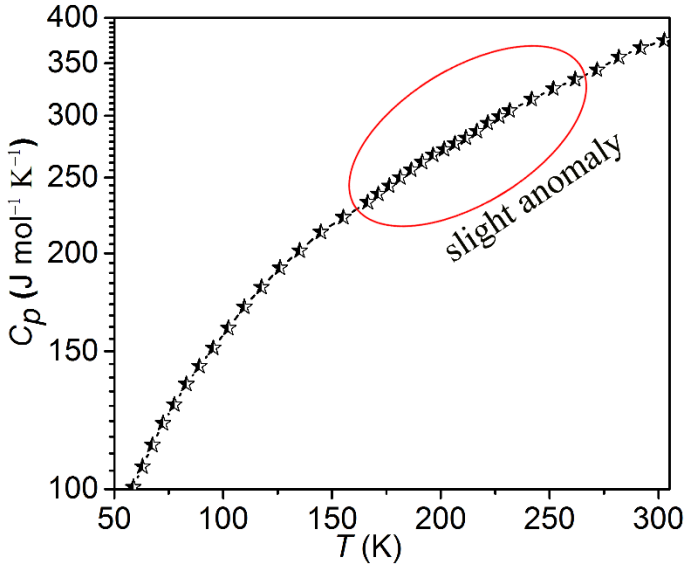

Figure S9. The C_p–T plot of **1** showing a slight anomaly between 150 and 270 K.

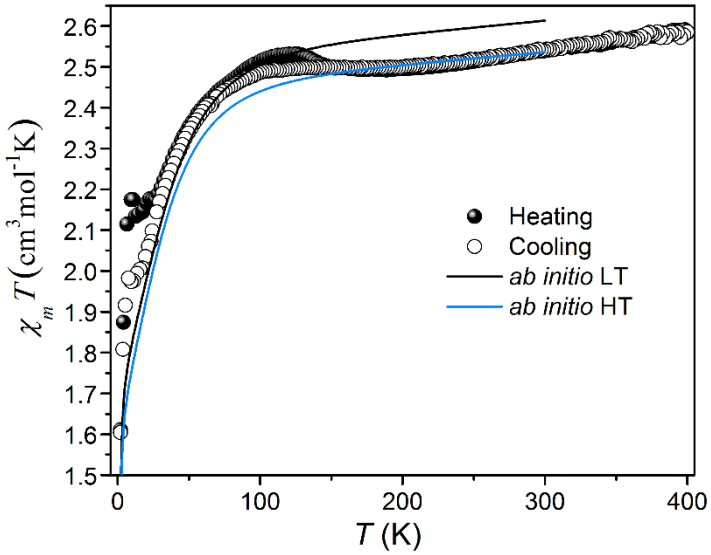

Figure S10. The $\chi_m T$–T plots of **1** during the cooling and heating cycle of 400–2–400 K.

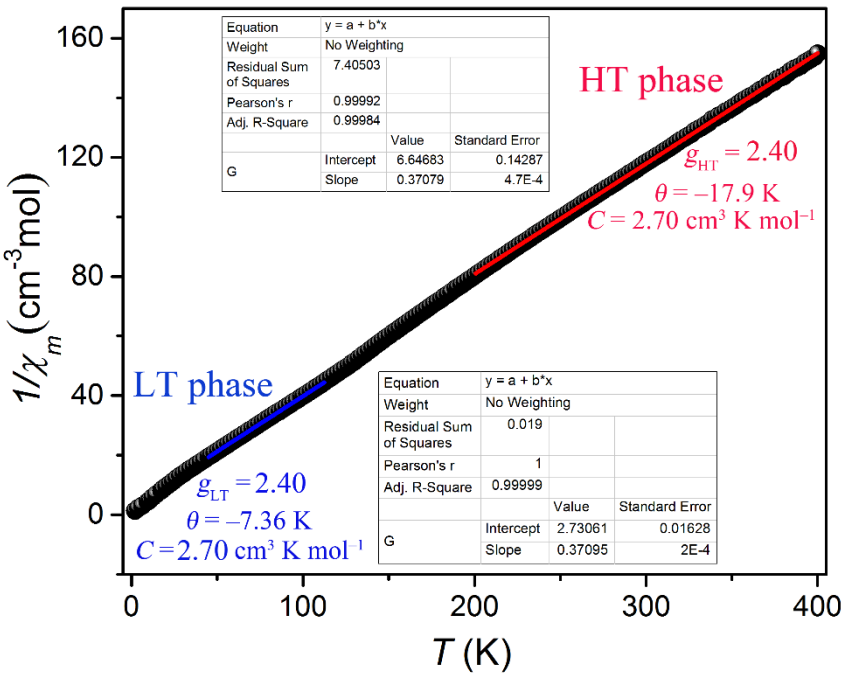

Figure S11. The $1/\chi_m$–T plot of **1** showing two different magnetism states in the HT and LT phases.

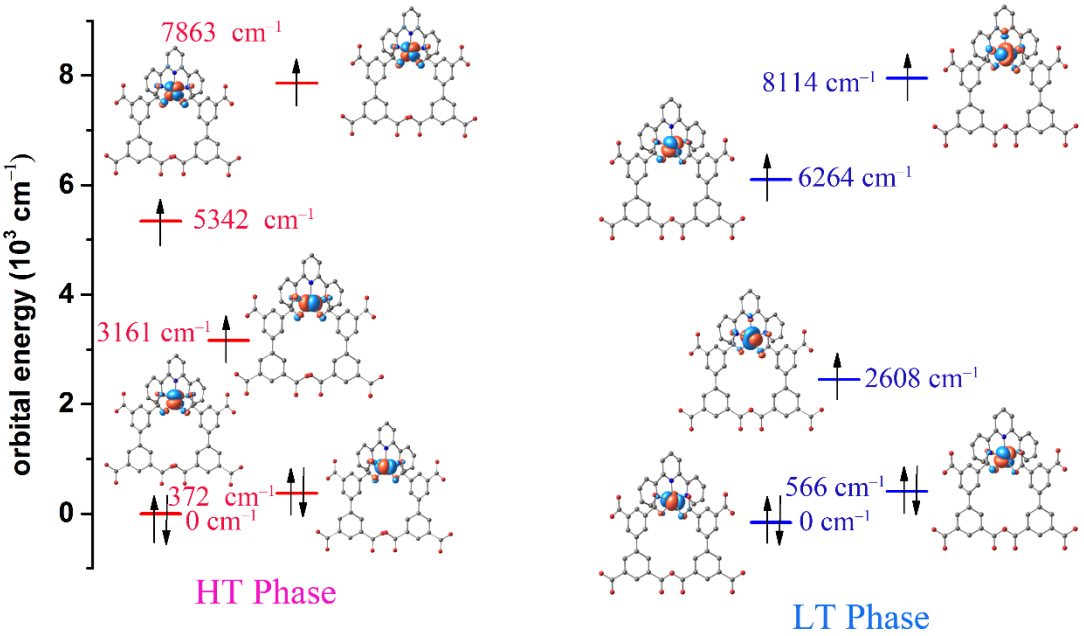

Figure S12. AILFT orbital diagrams showing the calculated orbital splitting in the HT phase (red) and the LT phase (blue). Horizontal lines depict orbital energies and arrows pointing up, or down stand for single electron spins. The first singly occupied *ab initio* ligand-field orbitals are accompanied by representations of their respective molecular orbitals.

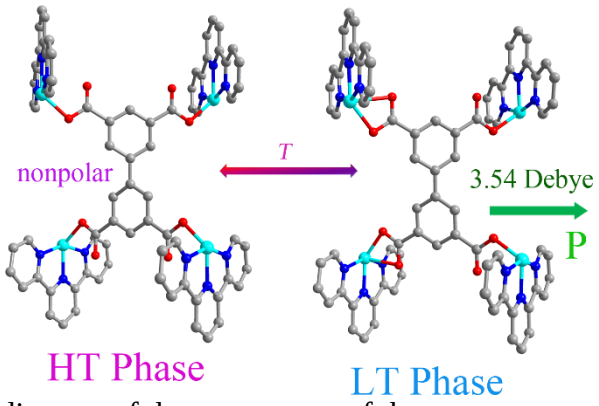

Figure S13. Schematic diagram of the appearance of the spontaneous polarization. The green arrow denotes the spontaneous polarization.

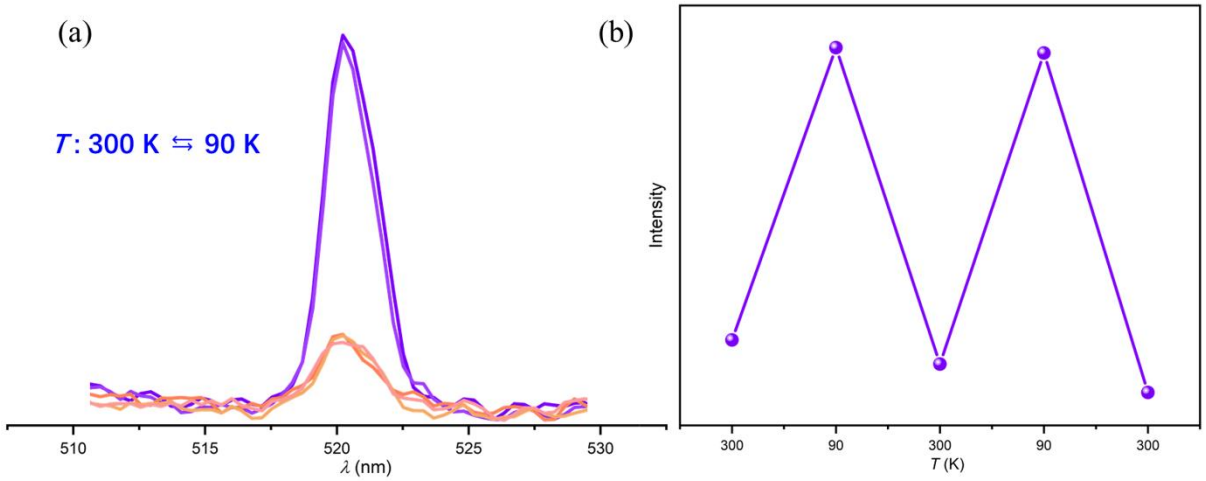

Figure S14. The (a) SHG signals and (b) SHG intensity of **1** under heating and cooling cycles between 300 K and 90 K.

S4. References

[S1]Lin X, Telepeni I, Blake AJ, Dailly A, Brown CM, Simmons JM, Zoppi M, Walker GS, Thomas KM, Mays TJ, Hubberstey P, Champness NR, Schröder M. *J Am Chem Soc*, 2009, 131: 2159−2171

[S2]Sheldrick G M. *Acta Cryst C*, 2015, 71: 3−8

[S3]Spek A. *J App Cryst*, 2003, 36: 7−13

[S4]Johnson ER, Keinan S, Mori-Sánchez P, Contreras-García J, Cohen AJ, Yang W. *J Am Chem Soc*, 2010, 132: 6498−6506

[S5]Lu T, Chen Q. *Chem Methods*, 2021, 1: 231−239

[S6]Frisch MJ, Trucks GW, Schlegel HB, Scuseria GE, Robb MA, Cheeseman JR, Scalmani G, Barone V, Petersson GA, Nakatsuji HL, Caricato MX, Marenich AV, Bloino J, Janesko BG, Gomperts R, Mennucci B, Hratchian HP, Ortiz JV, Izmaylov AF, Sonnenberg JL, Williams DF, Lipparini F, Egidi F, Goings J, Peng B, Petrone A, Henderson T, Ranasinghe D, Zakrzewski VG, Gao J, Rega N, Zheng G, Liang W, Hada M, Ehara M, Toyota K, Fukuda R, Hasegawa J, Ishida M, Nakajima T, Honda Y, Kitao O, Nakai H, Vreven T, Throssell K, Montgomery Jr JA, Peralta JE, Ogliaro F, Bearpark MJ, Heyd JJ, Brothers EN, Kudin KN, Staroverov VN, Keith TA, Kobayashi R, Normand J, Raghavachari K, Rendell AP, Burant JC, Iyengar SS, Tomasi J, Cossi M, Millam JM, Klene M, Adamo C, Cammi R, Ochterski JW, Martin RL, Morokuma K, Farkas O, Foresman JB, Fox DJ. Gaussian 16 Rev. B.01, Wallingford, CT. Gaussian 16 Rev. B.01, Wallingford, CT 2016

[S7]Neese F. *Rev Comp Mol Sci*, 2012, 2: 73–78

[S8]Neese F. *Rev Comp Mol Sci*, 2017, 8: e1327
[S9]Weigend F. Ahlrichs R. *Phys Chem Chem Phys*, 2005, 7: 3297–3305
[S10] Weigend F. *J Comput Chem*, 2008, 29: 167–175
[S11] Becke AD. *J Chem Phys*, 1993, 98: 5648–5652
[S12] Lee C, Yang W, Parr RG. *Phys Rev B*, 1988, 37: 785–789
[S13] Rechkemmer Y, Breitgoff FD, Meer MVD, Atanasov M, Hakl M, Orlita M, Neugebauer P, Neese F, Sarkar B, Slageren JV. *Nature Commun*, 2015, 7: 10467
[S14] Tang FS, Lin RB, Lin RG, Zhao JCG, Chen B. *J Solid State Chem*, 2018, 258: 346–350